POAC'17
Busan, KOREA

Proceedings of the 24th International Conference on
Port and Ocean Engineering under Arctic Conditions
June 11-16, 2017, Busan, Korea

Effective Tensile Strength of an Ice Sheet Using a Three-Dimensional FEM-DEM Approach

Ville-Pekka Lilja[1], Arttu Polojärvi[1], Jukka Tuhkuri[1], Jani Paavilainen[2]
[1] Aalto University, School of Engineering, Department of Mechanical Engineering, Finland
[2] Rand Simulation Ltd., Vantaa, Finland

ABSTRACT

A sea ice sheet may fail through several mechanisms when interacting with an obstacle. Susceptibility and mode of failure behave as functions of the physical size of a sheet. In this paper we compute the effective uniaxial tensile strength of an ice sheet for several different specimen sizes by applying a three-dimensional combined finite-discrete element approach. We evaluate the effect of the loading rate by using two displacement rates. Although a rate-independent cohesive formulation is used and the displacement rates applied are low, a significant rate effect emerges.

KEYWORDS: Ice; Combined FEM-DEM; Beam lattice network; Rate/size effect; Effective tensile strength

INTRODUCTION

Operating safely on ice-infested waters requires reliable knowledge of ice loads on structures. Information of ice-exerted loads can be obtained either through experimental campaigns or by using analytical or numerical methods. This paper investigates how an ice sheet modeled by using a three-dimensional combined finite-discrete element method (FEM-DEM) and meant to be used when conducting ice-structure interaction simulations, fractures while under uniaxial tension. We compute the effective uniaxial tensile strength of an ice sheet for several different specimen sizes. We evaluate the effect of the loading rate by using two displacement rates.

Failure of an ice sheet, using similar numerical methods, has been treated in the past by for example Hocking (1992), Jirásek & Bažant (1995), Hopkins (1998), Sayed & Timco (1998), Selvadurai & Sepehr (1999), Sand (2008), Paavilainen et al. (2009), Dorival et al. (2008), Konuk et al. (2009), Gürtner (2009), Kuutti et al. (2013), Lu et al. (2014), Herman (2016) and van den Berg (2016).

CONSTRUCTION OF THE NUMERICAL MODEL

The modeled ice sheet consists of a network of two-noded, three-dimensional co-rotational Timoshenko beam elements connected with the mass centroids of the overlaid undeformable discrete elements, Figure 1. Mesh is constructed by using centroidal Voronoi tessellation (CVT)

(Du et al., 1999). Mesh consists of convex polyhedra as the discrete elements and a Delaunay-triangulated network, or a lattice, of Timoshenko beam elements. Elasticity of an ice sheet is modeled solely with the beams, contacts between the broken pieces of ice by the discrete elements. The beam formulation follows closely Crisfield (1990,1997) while the contacts between the discrete elements are resolved as in Polojärvi et al. (2012). In essence, the model is a three-dimensional extension of our earlier two-dimensional FEM-DEM-model by Paavilainen et al. (2009) and was introduced by Paavilainen (2010). See Lilja et al. (2017) for additional details.

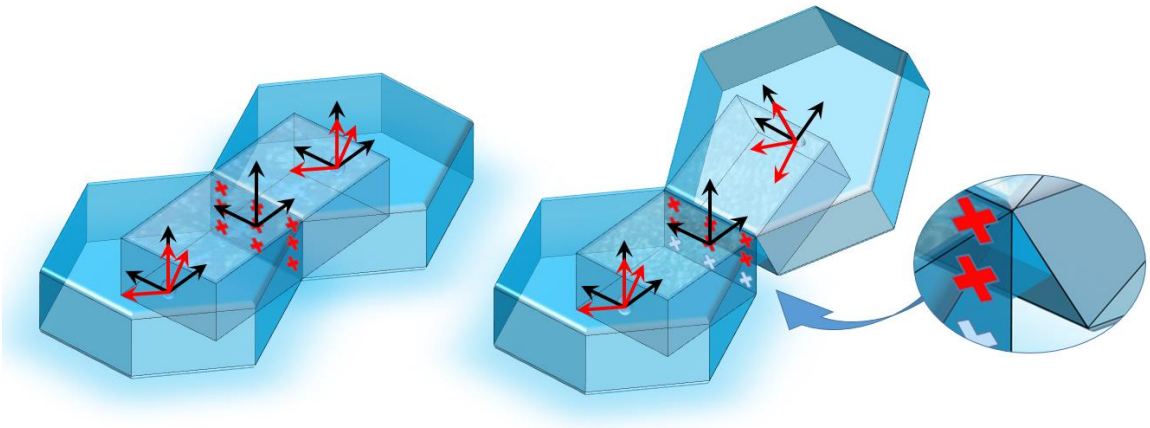

Figure 1. On the left: two discrete elements connected with a Timoshenko beam element. On the right: a partially fractured interface.

Description of Fracture

We use cohesive beam elements to model fracture. Cohesive sections are located at the mid-span of each beam element. Hooke's linearly elastic constitutive law, with a viscous damping model, is followed up until the onset of damage. When the cohesive cracking starts, a rate-independent linearly softening traction-separation law is activated and applied integration point wise to allow a crack to propagate along an interface between two adjacent discrete elements. As the constitutive model gets changed once the cohesive cracking initiates, approach is extrinsic (Seagraves & Radovitzky, 2010).

Numerical treatment of the softening process follows the model by Paavilainen et al. (2009). In their model a crack was able to propagate only vertically due to the modeling space being two-dimensional. As the model here is three-dimensional a crack is able to propagate both horizontally and vertically. Mixed mode fracture gets introduced by using the concept of an effective traction vector and representation of the state of stress with respect to a failure surface (Schreyer et al., 2006). Stress state calculation is done as with the numerical treatment of softening plasticity and includes a radial return mapping algorithm. Simpson's two-dimensional (composite) numerical integration rule is used in integrating the internal force and moment resultants.

Description of fracture using cohesive elements, when the crack path is not known in advance, is not energetically convergent with any reasonable number of elements used (Seagraves, 2013). If a mesh is structured, crack growth is also prone to preferred directions as the artificial toughness induced by the mesh varies with direction. Using a CVT-based mesh renders the crack growth isotropic. CVT-tessellated meshes are isotropic although the mesh induced toughness is still artificially high (Leon et al., 2014; Spring et al., 2014; Rimoli & Rojas, 2015).

SIMULATIONS

Main goals of our simulations are: (1) to compute the effective uniaxial tensile strength of an ice sheet for several different specimen sizes and (2) to evaluate the effect of the loading rate. A set of square-shaped sheets having a size range of 1:16 was, thus, created for the tests, Figure 2. Sheets had the side lengths of L = 10, 20, 40, 80 and 160 m and the thicknesses of h = 0.5, 1.0 and 1.5 m. For each sheet, we used two mesh densities: a mesh with an average discrete element size of $l = 2h$ and a mesh with an average discrete element size of $l = 3h$. Each broken fragment should have, thus, in minimum, a size that is comparable with actual block sizes measured from ridge sails (Kankaanpää, 1988; Høyland, 2007; Kulyakhtin, 2014). Ten randomized CVT-meshes were created for all of the sheets, excluding the sheet with L=160 m, h = 0.5 m and $l = 2h$, for which six meshes were produced.

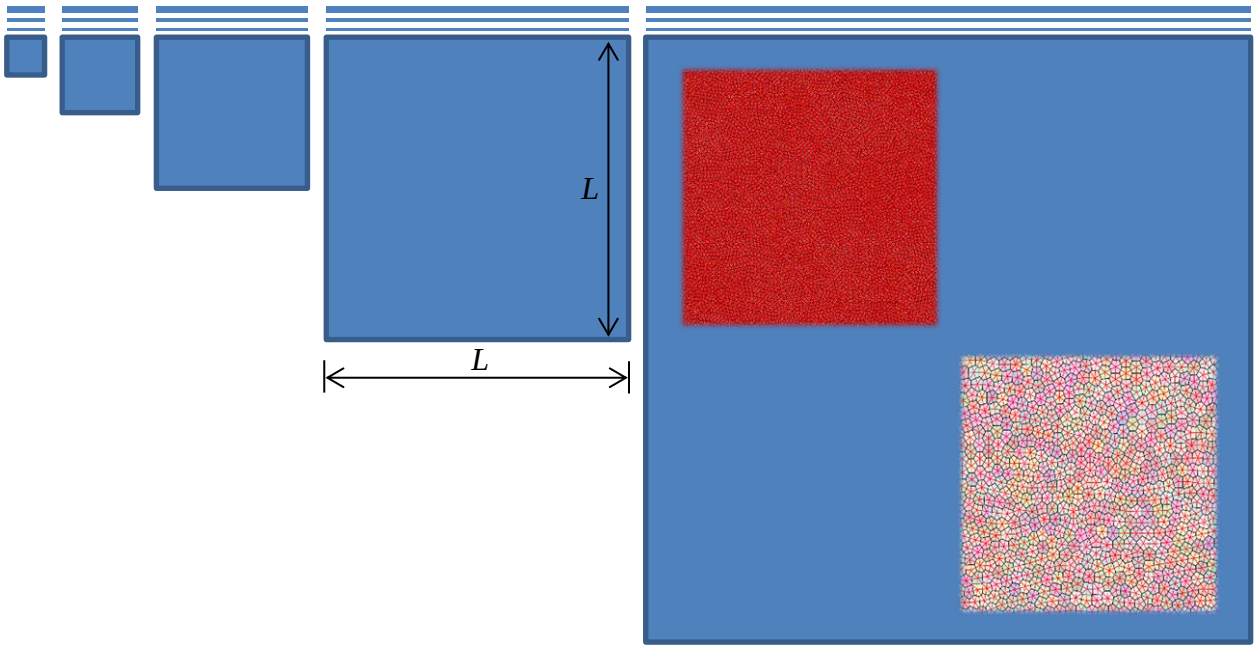

Figure 2. Size range (1:16) of the ice sheets considered. From left to right: L = 10, 20, 40, 80 and 160 m. The largest sheet on the right shows also sections of the two meshes that have the most and the least amount of discrete elements for that size: 29561 discrete elements (h = 0.5 m, $l = 2h$) and 1460 discrete elements (h = 1.5 m, $l = 3h$).

Effective Tensile Strength

Effective tensile strength was computed via a uniaxial tensile test. Each sheet was loaded under displacement control using two displacement rates: $v = 0.1$ m/s and 0.01 m/s, as shown in Figure 3. Nodes on the right and on the left boundaries were pulled into the positive and the negative X-directions, respectively, until the sheet was completely fractured. To prevent early fracture near the boundaries, a linearly changing initial velocity field $v_X = 2vX/L$ was applied, as described by Miller et al. (1999). No other constraints were used. Post-fracture contacts were not considered.

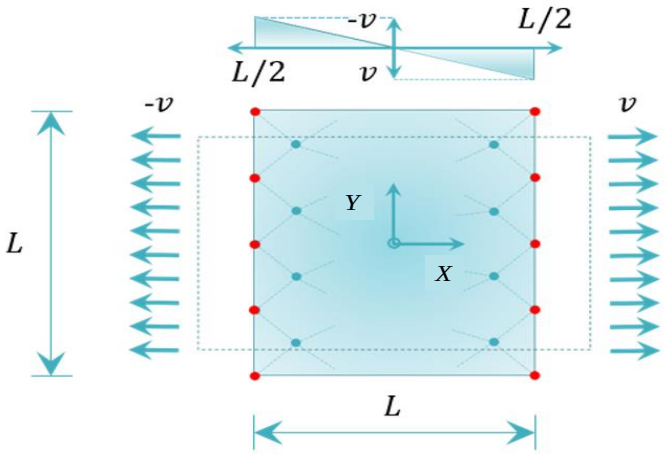

Figure 3. Boundary conditions and the initial velocity field used in the computation of the effective tensile strength.

Effective tensile strength was calculated for each sheet through $\sigma_{TS} = F_X/A_0$, where F_X is the maximum resultant force in the X-direction and $A_0 = Lh$ is the initial cross-sectional area of each sheet. The resultant force F_X was calculated for each sheet by summing up the X-direction components of the internal nodal force vectors of the beams having nodes either on the right or on the left boundary. Table 1 shows the main parameters of the simulations.

Table 1. Main parameters used in the simulations.

Parameter	Symbol	Unit	Value
Young's modulus	E^b	GPa	4
Poisson's coefficient	ν		0.3
Density of ice	ρ_{ice}	kg/m^3	920
Damping constant	c		critical[1]
Time step	Δt	s	1.0×10^{-5}…5.0×10^{-5}
Critical axial/shear stress	σ_b / τ_b	MPa	0.125
Specific fracture energy	G_f	J/m^2	15

[1] $c = \sqrt{m_{eff}E^b}$, where m_{eff} is the average of the masses of the two discrete elements a beam connects.

Results

Figures 4 and 5 show (with the displacement rates: $v = 0.1$ m/s and $v = 0.01$ m/s, respectively) the computed effective average tensile strengths σ_{TS} and their standard deviations in an order of ascending sheet size *L*. For each *L* the results are arranged in an order of ascending sheet thickness *h* and the discrete element size *l* (for each *h*). Results are the averages calculated using ten randomized CVT-meshes, except for the case with *L*=160 m, *h* = 0.5 m and *l* = 2*h*, for which six meshes were used.

With the displacement rate $v = 0.1$ m/s, the effective tensile strength σ_{TS} grows as a function of sheet thickness *h* and decreases as a function of sheet size *L*. For the two smallest sheet sizes the differences between the results, whether a discrete element size of either *l* = 2*h* or *l* = 3*h* is used, are large. Sheets that are smaller, thicker or meshed with a discrete element size of *l* = 3*h* have a higher effective tensile strength. Except for the smallest sheet size, the deviations are observed to be small. The ratio $\sigma_{\mathrm{TS}}/\sigma_{\mathrm{b}}$ between the computed effective tensile strength of an ice sheet and the critical axial stress as used with the beams varies from approximately 5.74 for the smallest and the thickest sheets (*L* = 10 m, *h* = 1.5 m, *l* = 3*h*) to an average of 0.97 for the largest sheets.

With the displacement rate $v = 0.01$ m/s, the effective tensile strength σ_{TS} decreases as a function of sheet size *L*. For the sheets with *L* = 10 m or *L* = 20 m, the effective tensile strength grows as a function of sheet thickness *h*. The sheets with *L* = 40 m produce (practically) equal results for all of the cases. For the sheets with *L* = 80 m or *L* = 160 the tensile strength decreases as a function of sheet thickness *h*. Except for the smallest sheet size, the deviations are observed to be small. The ratio $\sigma_{\mathrm{TS}}/\sigma_{\mathrm{b}}$ varies from approximately 1.18 for the smallest and the thickest sheets to an average of 0.81 for the largest sheets.

Although a rate-independent cohesive formulation is used and the displacement rates applied are low, a significant rate effect emerges. Ratio between the maximum effective tensile strengths of the smallest and the thickest sheets, for the two displacement rates considered, is approximately 4.9 and reduces to an average value of approximately 1.2 for the largest sheets.

As an example, a fractured ice sheet with *L* = 160 m, *h* =0.5 m, *l* = 2*h* (29561 discrete elements), and loaded with a displacement rate $v = 0.1$ m/s, is shown in Figure 5. Broad areas become cohesive and are highlighted in purple. Several fully grown cracks appear and are highlighted in gray. Areas remaining elastic are highlighted in blue. Cracks tend to branch, bridge and have a tortuous pattern.

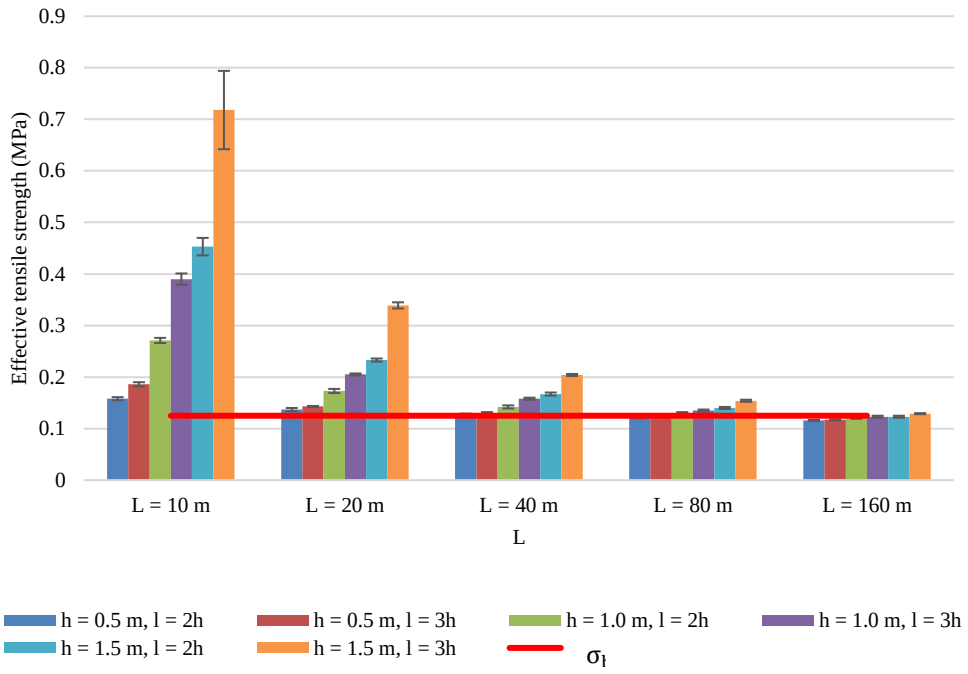

Figure 4. Effective tensile strength σ_{TS} as a function of sheet size L, sheet thickness h and discrete element size l. Displacement rate used: $v = 0.1$ m/s. Critical axial stress σ_b, as used with the beams, is highlighted with a red horizontal line.

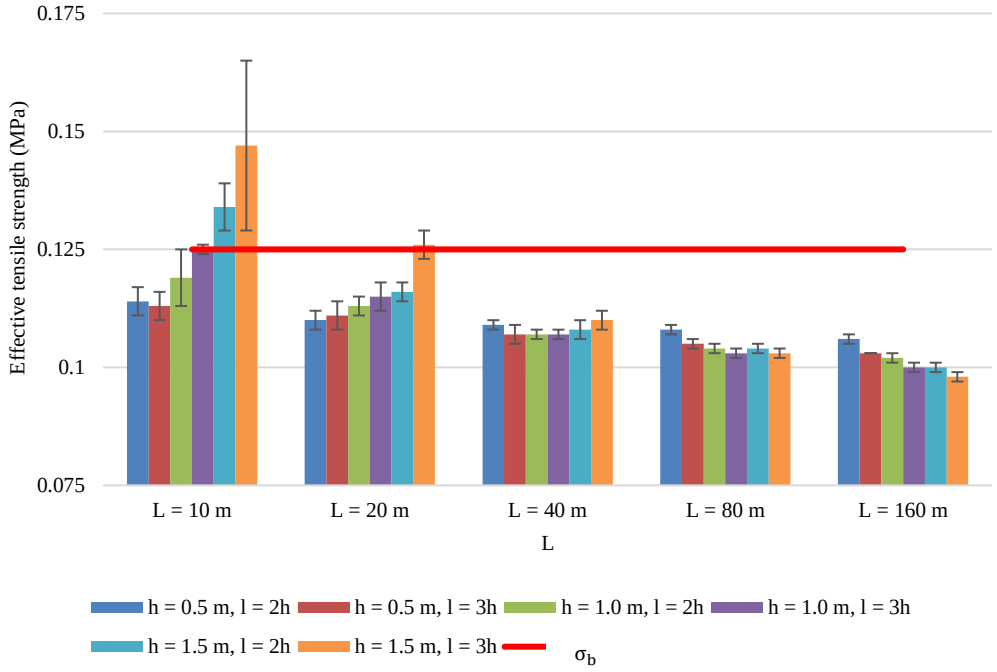

Figure 5. Effective tensile strength σ_{TS} as a function of sheet size L, sheet thickness h and discrete element size l. Displacement rate used: $v = 0.01$ m/s. Critical axial stress σ_b, as used with the beams, is highlighted with a red horizontal line.

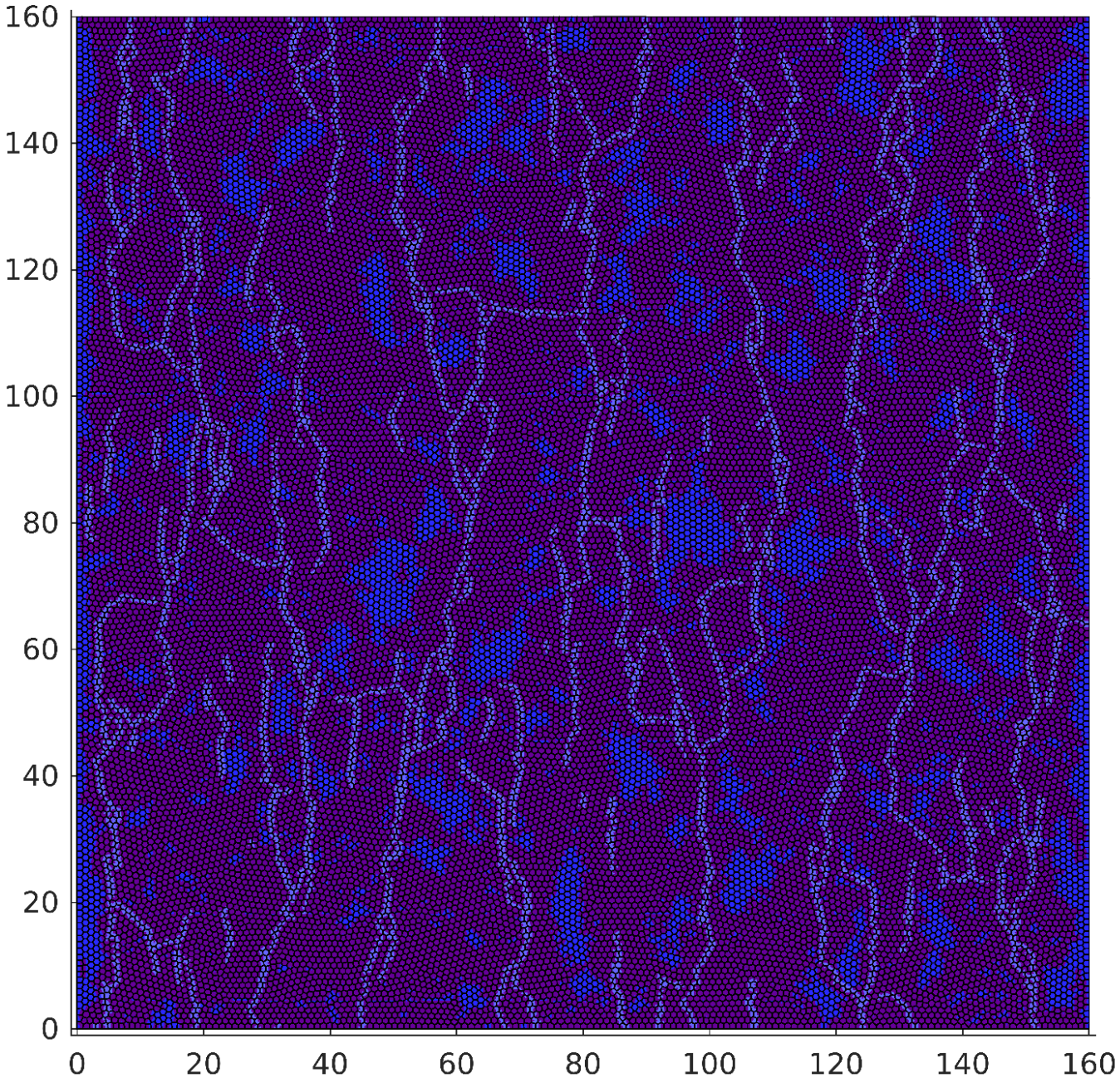

Figure 6. A fractured ice sheet with L = 160 m, h =0.5 m and l = 2h (29561 discrete elements). Completely fractured beams are highlighted in gray, partially fractured (cohesive) beams in purple and elastic beams in blue. Sheet was loaded in tension in the horizontal direction with a displacement rate $v = 0.1$ m/s.

CONCLUSIONS

We computed the effective uniaxial tensile strength of an ice sheet modeled by using a three-dimensional FEM-DEM approach for several different specimen sizes. Model consists of rigid discrete elements combined with co-rotational, viscously damped, cohesive Timoshenko beam elements. Centroidal Voronoi tessellation (CVT) was used to create the meshes. Effect of the loading rate was evaluated by using two displacement rates: $v = 0.1$ m/s and $v = 0.01$ m/s.

With the displacement rate $v = 0.1$ m/s the effective tensile strength σ_{TS} grows as a function of sheet thickness *h* and decreases as a function of sheet size *L*. For the smallest sheet size the differences between the results, whether a discrete element size of either $l = 2h$ or $l = 3h$ is used, are large. Sheets that are smaller, thicker or meshed with a discrete element size of $l = 3h$ have a higher effective tensile strength. The ratio $\sigma_{\mathrm{TS}}/\sigma_{\mathrm{b}}$ between the computed effective tensile strength and the critical axial stress as used with the beams varies from approximately 5.74 for the smallest and the thickest sheets (L = 10 m, h = 1.5 m, $l = 3h$) to an average of 0.97 for the largest sheets.

With the displacement rate $v = 0.01$ m/s the effective tensile strength σ_{TS} decreases as a function of sheet size *L*. For the sheets with *L* = 10 m or *L* = 20 m, the effective tensile strength grows as a function of sheet thickness *h*. The sheets with *L* = 40 m produced (practically) equal results for all of the cases. For the sheets with *L* = 80 m or *L* = 160 the effective tensile strength decreases as a function of the sheet thickness *h*. The ratio $\sigma_{\mathrm{TS}}/\sigma_{\mathrm{b}}$ varies from approximately 1.18 for the smallest and the thickest sheets to an average of 0.81 for the largest sheets.

Although a rate-independent cohesive formulation is used and the displacement rates applied are low, a significant rate effect emerges. Ratio between the maximum effective tensile strengths of the smallest and the thickest sheets, with the two displacement rates considered, is approximately 4.9 and reduces to an average value of approximately 1.2 for the largest sheets.

ACKNOWLEDGEMENTS

Authors gratefully acknowledge the financial support by the Academy of Finland through the project: “Discrete Numerical Simulation and Statistical Analysis of the Failure Process of a Non-homogeneous Ice Sheet Against an Offshore Structure.”

REFERENCES

Crisfield, M. A., 1990. A consistent co-rotational formulation for non-linear, three-dimensional, beam-elements. *Computer methods in applied mechanics and engineering,* Volume 81, pp. 131-150.

Crisfield, M. A., 1997. chs. 17.1-2. In: *Non-linear Finite Element Analysis of Solids and Structures, volume 2: Advanced Topics.* New York: John Wiley & Sons Ltd., pp. 213-232.

Dorival, O., Metrikine, A. & Simone, A., 2008. *A lattice model to simulate ice-structure interaction.* ASME 2008 27th International Conference on Offshore Mechanics and Arctic Engineering, Estoril, Portugal, pp. 989-996.

Du, Q., Faber, V. & Gunzburger, M., 1999. Centroidal Voronoi Tessellations: Applications and Algorithms. *SIAM Review,* Volume 41, p. 637–676.

Gürtner, A., 2009. *Experimental and Numerical Investigations of Ice-Structure Interaction,* Doctoral thesis, Norwegian University of Science and Technology, NTNU: Trondheim.

Herman, A., 2016. Discrete-Element bonded-particle Sea Ice model DESIgn, version 1.3a – model description and implementation. *Geoscientific Model Development,* Volume 9, p. 1219–1241.

Hocking, G., 1992. The discrete element method for analysis of fragmentation of discontinua. *Engineering Computations,* Volume 9, pp. 145 - 155.

Hopkins, M., 1998. Four stages of pressure ridging. *Journal of geophysical research,* Volume 103, pp. 21883-21891.

Høyland, K. V., 2007. Morphology and small-scale strength of ridges in the North-Western Barents Sea. *Cold Regions Science and Technology,* Volume 48, pp. 169-187.

Jirásek, M. & Bažant, Z. P., 1995. Particle Model for Quasibrittle Fracture and Application to Sea Ice. *Journal of Engineering Mechanics,* Volume 121, pp. 1016-1025.

Kankaanpää, P., 1988. Morphology of sea ice pressure ridges in the Baltic Sea. *Geophysica,* Volume 24, pp. 15-44.

Konuk, I., Gürtner, A. & Yu, S., 2009. *A Cohesive Element Framework for Dynamic Ice-Structure Interaction Problems - Part I: Review and Formulation.* ASME 2009 28th International Conference on Ocean, Offshore and Arctic Engineering, Honolulu, Hawaii, USA, May 31 - June 5, pp. 33-41.

Kulyakhtin, S., 2014. *Distribution of Ice Block Sizes in Sails of Pressure Ice Ridges.* Singapore, August 11 to 15, 22nd IAHR International Symposium on Ice.

Kuutti, J., Kolari, K. & Marjavaara, P., 2013. Simulation of ice crushing experiments with cohesive surface methodology. *Cold Regions Science and Technology,* Volume 92, pp. 17-28.

Leon, S. E., Spring, D. W. & Paulino, G. H., 2014. Reduction in mesh bias for dynamic fracture using adaptive splitting of polygonal finite elements. *International Journal of Numerical Methods in Engineering,* Volume 100, pp. 555-576.

Lilja, V. P., Polojärvi, A., Tuhkuri, J. & Paavilainen, J., 2017. *A three-dimensional FEM-DEM model of an ice sheet.* Busan, Korea, June 11-16, Proceedings of the 24th International Conference on Port and Ocean Engineering under Arctic Conditions.

Lu, W., Lubbad, R. & Løset, S., 2014. Simulating Ice-Sloping Structure Interactions With the Cohesive Element Method. *Journal of Offshore Mechanics and Arctic Engineering,* Volume 136, pp. 1-16.

Miller, O., Freund, L. B. & Needleman, A., 1999. Modeling and simulation of dynamic fragmentation in brittle materials. *International Journal of Fracture,* Volume 96, pp. 101-125.

Paavilainen, J., 2010. Jäälautan murtuminen kartiorakennetta vasten. In: J. Heinonen, ed. *Jatkuvan murtumisprosessin mallinnus jää-rakenne vuorovaikutusprosessissa,* Research - report (in Finnish), project: "STRUTSI". Technical Research Center of Finland, VTT: Espoo, pp. 25-27.

Paavilainen, J., Tuhkuri, J. & Polojärvi, A., 2009. 2D combined finite-discrete element method to model multi-fracture of beam structures. *Engineering computations,* Volume 26, pp. 578-598.

Polojärvi, A., Tuhkuri, J. & Korkalo, O., 2012. Comparison and analysis of experimental and virtual laboratory scale punch through tests. *Cold Regions Science and Technology,* Volume 81, pp. 11-25.

Rimoli, J. J. & Rojas, J. J., 2015. Meshing strategies for the alleviation of mesh-induced effects in cohesive element models. *International Journal of Fracture,* Volume 193, pp. 29-42.

Sand, B., 2008. *Nonlinear finite element simulations of ice forces on offshore structures,* Doctoral thesis, Luleå University of Technology: Luleå.

Sayed, M. & Timco, G., 1998. *A Lattice Model of Ice Failure,* National Research Council of Canada: Ottawa.

Schreyer, H. L. et al., 2006. Elastic-decohesive constitutive model for sea ice. *Journal of geophysical research,* Volume 111, pp. 1-21.

Seagraves, A. N., 2013. *Next generation computational tools for extreme-scale simulation of dynamic fracture and fragmentation in three dimensions,* Ph.D. dissertation, Massachusetts Institute of Technology: Cambridge.

Seagraves, A. & Radovitzky, R., 2010. Advances in Cohesive Zone Modeling of Dynamic Fracture. In: A. Shukla, G. Ravichandran & Y. D. S. Rajapakse, eds. *Dynamic Failure of Materials and Structures.* Springer Science: U.S.A, pp. 349-405.

Selvadurai, A. P. S. & Sepehr, K., 1999. Two-dimensional discrete element simulations of ice-structure interaction. *International Journal of Solids and Structures,* Volume 36, pp. 4919-4940.

Spring, D. W., Leon, S. E. & Paulino, G. H., 2014. Unstructured polygonal meshes with adaptive refinement for the numerical simulation of dynamic cohesive fracture. *International Journal of Fracture,* Volume 189, pp. 33-57.

van den Berg, M., 2016. *A 3-D Random Lattice Model of Sea Ice.* Arctic Technology Conference, St. John’s, Newfoundland and Labrador, Canada, 24-26 October.